

Lehmann representation of the nonequilibrium self-energy

Christian Gramsch^{1,2} and Michael Potthoff^{1,2}

¹*Institute for Theoretical Physics, University of Hamburg, Jungiusstraße 9, 20355 Hamburg, Germany*

²*The Hamburg Centre for Ultrafast Imaging, Luruper Chaussee 149, 22761 Hamburg, Germany*

It is shown that the nonequilibrium self-energy of an interacting lattice-fermion model has a unique Lehmann representation. Based on the construction of a suitable non-interacting effective medium, we provide an explicit and numerically practicable scheme to construct the Lehmann representation for the self-energy, given the Lehmann representation of the single-particle nonequilibrium Green's function. This is of particular importance for an efficient numerical solution of Dyson's equation in the context of approximations where the self-energy is obtained from a reference system with a small Hilbert space. As compared to conventional techniques to solve Dyson's equation on the Keldysh contour, the effective-medium approach allows to reach a maximum propagation time which can be several orders of magnitude longer. This is demonstrated explicitly by choosing the nonequilibrium cluster-perturbation theory as a simple approach to study the long-time dynamics of an inhomogeneous initial state after a quantum quench in the Hubbard model on a 10×10 square lattice. We demonstrate that the violation of conservation laws is moderate for weak Hubbard interaction and that the cluster approach is able to describe prethermalization physics.

PACS numbers: 71.10.-w, 71.10.Fd, 67.85.Lm, 78.47.J-

I. INTRODUCTION

The study of physical phenomena that arise in strongly correlated systems far from equilibrium has become a field of highly active research recently.^{1,2} For the theoretical description of such systems, Green's-function-based approaches starting from the Keldysh formalism³ have proven to be very useful. A number of different approximation schemes rely on this concept.⁴⁻¹¹ Central to these approaches is the self-energy which is related to the one-particle Green's function through Dyson's equation. However, while the numerical solution of Dyson's equation is rather straightforward in the equilibrium case, the computational effort is considerably increased for systems out of equilibrium since operations with matrices depending on two independent contour time variables typically scale cubically in the number of time steps. Apart from other challenges characteristic for the respective approach, already this scaling poses a severe limit on the maximal reachable propagation time in a numerical calculation. Applying additional concepts or approximations, such as the generalized Kadanoff-Baym ansatz^{12,13} or exploiting a rapid decay of the memory,¹⁴ are necessary to overcome this limitation.

It was proposed recently¹⁵ that it can be advantageous to avoid the direct inversion of Dyson's equation by applying a mapping onto a Markovian propagation scheme. To this end it is necessary to *assume* the existence of a certain functional form for the nonequilibrium self-energy, namely the existence of a Lehmann representation.

In the present paper we explicitly construct this Lehmann representation. With this at hand, we pick up the proposed idea to solve Dyson's equation by means of a Markovian propagation and exploit the fact that the Lehmann representation of the exact self-energy of a small reference system has a finite number of terms only. This allows us to solve Dyson's equation with an effort that scales linearly in the maximum propagation time t_{\max} .

For equilibrium Green's functions, the Lehmann representation is a well established concept.¹⁶ It uncovers the ana-

lytical properties of the Green's function and can be used to show that the related spectral function is positive definite. It is further essential for the evaluation of diagrams through contour integrations in the complex frequency plane, for the derivation of sum rules, etc. The generalization of the Lehmann representation to nonequilibrium Green's function is straightforward.¹⁷ Applications include nonequilibrium dynamical mean-field theory (DMFT) where it allows for a Hamiltonian-based formulation of the impurity problem.¹⁷

The explicit construction of a Lehmann representation for the *self-energy*, on the other hand, turns out to be more tedious, already for the equilibrium case: In a recent work such a construction was worked out¹⁸ from a diagrammatic perspective and used to cure the problem of possibly negative spectral functions arising from a summation of a subclass of diagrams.

Here, we address the nonequilibrium self-energy of a general, interacting lattice-fermion model: (i) We rigorously show the existence of the Lehmann representation by presenting an explicit construction scheme that is based on the Lehmann representation of the nonequilibrium Green's function. (ii) Using a simple example, namely the cluster-perturbation theory^{7,9,19-22} (CPT), we furthermore demonstrate that the Lehmann representation of the self-energy can in fact be implemented numerically and used to study the time evolution of a locally perturbed Hubbard model on a large square lattice (10×10 sites). Propagation times of several orders of magnitude in units of the inverse hopping amplitude can be reached with modest computational resources. (iii) While the CPT approximation for the self-energy is rather crude and shown to violate a number of conservation laws, it is possible with this approximation to study the weak-coupling limit of the Hubbard model in a reasonable way. In particular we demonstrate that prethermalization physics is already captured on this level.

The paper is organized as follows: In Section II we briefly discuss the generalization of the Lehmann representation to nonequilibrium Green's functions. The main idea of Ref. 15

about the Markovian propagation scheme is recalled in Sec. III A. The explicit construction scheme for the nonequilibrium self-energy is outlined in Section III B. Section IV is devoted to the application of our formalism to the cluster-perturbation theory. Sec. V presents numerical results for the time evolution of a local perturbation in the fermionic Hubbard model. We conclude the paper with a summary and an outlook in Sec. VI.

II. LEHMANN REPRESENTATION OF THE ONE-PARTICLE GREEN'S FUNCTION

We consider an arbitrary, fermionic model Hamiltonian

$$H(t) = \sum_{ij} (T_{ij}(t) - \delta_{ij}\mu) c_i^\dagger c_j + \frac{1}{2} \sum_{ijj'} U_{ijj'} c_i^\dagger c_j^\dagger c_j c_j, \quad (1)$$

where the indices i, j run over the possible one-particle orbitals (lattice sites, local orbitals, spin projection, ...). Fermions in such states are created (annihilated) by the operators c_i^\dagger (c_i). At time $t = 0$, the system with Hamiltonian $H(0) = H_{\text{ini}}$ is assumed to be in thermal equilibrium with inverse temperature β and chemical potential μ . Nonequilibrium real-time dynamics for $t > 0$ is initiated by the time dependence of the one-particle or the interaction parameters. This covers challenging experimental setups such as time-resolved photoemission spectroscopy²³ or experiments with ultracold gases in optical lattices.²⁴

The one-particle Green's function is given by

$$G_{ij}(t, t') = -i \langle \mathcal{T}_C \hat{c}_i(t) \hat{c}_j^\dagger(t') \rangle_H \\ \equiv \frac{-i}{Z} \text{tr} \left(\exp(-\beta H_{\text{ini}}) \left[\mathcal{T}_C \hat{c}_i(t) \hat{c}_j^\dagger(t') \right] \right), \quad (2)$$

where “tr(...)” traces over the Fock space, i.e., we take averages using the grand-canonical ensemble. $Z = \text{tr}(\exp(-\beta H_{\text{ini}}))$ defines the grand-canonical partition function and \mathcal{T}_C the time-ordering operator on the L-shaped Keldysh-Matsubara contour C (see Fig. 1). The time variables t and t' are understood as contour times that can lie on the upper, lower or Matsubara branch of C . We further introduce the convention that operators with a hat carry a time dependence according to the Heisenberg picture, i.e., $\hat{c}_i(t) = U^\dagger(t, 0) c_i U(t, 0)$, where $U(t, t') = \mathcal{T} \exp(-i \int_{t'}^t H(t_1) dt_1)$ is the system's time-evolution operator and \mathcal{T} the time-ordering operator. An in-depth introduction to the Keldysh formalism³ can be found in Refs. 25, 26.

As has been shown in Ref. 17, the one-particle Green's function can be cast into the form

$$G_{ij}(t, t') = \sum_{\alpha} Q_{i\alpha}(t) g(\varepsilon_{\alpha}; t, t') Q_{j\alpha}^*(t'), \quad (3)$$

which we will call its Lehmann representation in the following. $g(\varepsilon; t, t')$ is the non-interacting Green's function of an isolated one-particle mode ($h_{\text{mode}} = \varepsilon c^\dagger c$) with excitation energy ε :

$$g(\varepsilon; t, t') = i [f(\varepsilon) - \Theta_C(t, t')] e^{-i\varepsilon(t-t')}. \quad (4)$$

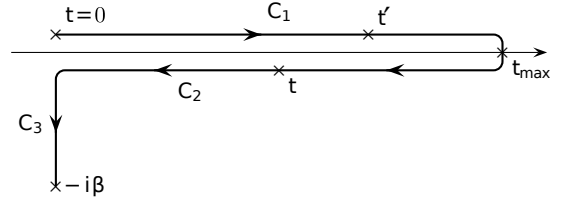


FIG. 1: Keldysh-Matsubara contour C . C_1 denotes the upper branch, C_2 the lower branch and C_3 the Matsubara branch. In the shown example t is later than t' in sense of the contour, denoted as $t >_C t'$ in the text.

Here, $f(\varepsilon) = (e^{\beta\varepsilon} + 1)^{-1}$ denotes the Fermi-function while $\Theta_C(t, t')$ refers to the contour variant of the Heaviside step function ($\Theta_C(t, t') = 1$ for $t \geq_C t'$, $\Theta_C(t, t') = 0$ otherwise). $Q(t)$ is defined to be equal on the upper and lower branch of the contour and furthermore constant on the Matsubara branch with $Q(-i\tau) = Q(0)$ and $\tau \in [0, \beta]$. If the eigenstates $|m\rangle$ of the initial Hamiltonian (i.e., $H_{\text{ini}}|m\rangle = E_m|m\rangle$) are used as a basis for tracing over the Fock space in Eq. (2), one has

$$Q_{i\alpha}(t) = Q_{i(m,n)}(t) = z_{(m,n)} \langle m | \hat{c}_i(t) | n \rangle e^{i\varepsilon_{(m,n)} t}, \quad (5)$$

where $z_{(m,n)} = \sqrt{(e^{-\beta E_m} + e^{-\beta E_n})/Z}$ and where the superindex $\alpha = (m, n)$ labels the possible one-particle excitations with corresponding excitation energies $\varepsilon_{\alpha} = \varepsilon_{(m,n)} = E_n - E_m$. Note that this definition of $Q(t)$ indeed satisfies $Q(-i\tau) = Q(0)$. We emphasize that Q as a matrix is not quadratic. Our expression can be seen as a direct generalization of the time-independent Q -matrix discussed in Ref. 27. We further note that the rows of the Q -matrix fulfill the orthonormality condition

$$[Q(t)Q^\dagger(t)]_{ij} = \sum_{\alpha} Q_{i\alpha}(t) Q_{j\alpha}^*(t) = \langle \{ \hat{c}_i(t), \hat{c}_j^\dagger(t) \} \rangle_H = \delta_{ij}, \quad (6)$$

where $\{A, B\} = AB + BA$ denotes the anticommutator.

III. LEHMANN REPRESENTATION OF THE SELF-ENERGY

A. Motivation

In several Green's-function-based methods, an approximate self-energy Σ' is obtained from a small reference system using exact diagonalization. The desired one-particle Green's function G of a much larger system is then obtained through Dyson's equation

$$G_{ij}(t, t') = [G_0]_{ij}(t, t') \\ + \int_C \int_C dt_1 dt_2 \sum_{k_1 k_2} [G_0]_{ik_1}(t, t_1) \Sigma'_{k_1 k_2}(t_1, t_2) G_{k_2 j}(t_2, t'), \quad (7)$$

where G_0 denotes the non-interacting Green's function (i.e., $U = 0$) of the model given by Eq. (1). Typical examples include dynamical mean-field theory (DMFT),^{5,6,28,29}

where Σ' is obtained from a single-impurity Anderson model,¹⁷ or cluster-perturbation^{7,9,19–22} and self-energy functional theory,^{10,30,31} where Σ' stems from a small reference system. To solve Eq. (7) numerically, a discretization of the continuous time-contour C is necessary. The number of time steps required to reach a given maximal time is dependent on the lowest relevant timescale that is set by a given Hamiltonian. Based on this discretization, the effort required to solve Eq. (7) for G scales cubically in the number of time steps and also the system size. Despite this challenge also the memory consumption, which scales quadratically in these quantities, poses a problem. Progress was made recently¹⁵ by introducing a mapping of Eq. (7) onto a Markovian propagation-scheme.

The idea proposed by the authors of Ref. 15 relies on the *assumption* that the self-energy can be written in the following form:

$$\Sigma'_{ij}(t, t') = \delta_C(t, t') \Sigma'_{ij}{}^{\text{HF}}(t) + \sum_s h_{is}(t) g(h_{ss}; t, t') h_{js}^*(t). \quad (8)$$

Here, $\Sigma'_{ij}{}^{\text{HF}}(t)$ denotes the time-local Hartree-Fock term. This decomposition is very similar to the expression Eq. (3) for the Green's function. We will refer to this as the Lehmann representation of the self-energy. The immediate and important advantage of the Lehmann representation is that the self-energy can be interpreted as a hybridization function.^{15,17} This property allows to write down an effective non-interacting model with Hamiltonian

$$H_{\text{eff}}(t) = \sum_{ij} (T_{ij}(t) + \Sigma'_{ij}{}^{\text{HF}}(t)) c_i^\dagger c_j + \sum_{is} (h_{is}(t) c_i^\dagger a_s + \text{h.c.}) + \sum_s h_{ss} a_s^\dagger a_s. \quad (9)$$

The s -degrees of freedom represent “virtual” orbitals in addition to the physical degrees of freedom labeled by i . They form an “effective medium” with on-site energies h_{ss} and hybridization strengths $h_{is}(t)$ such that the *interacting* Green's function of the original model is the same as the Green's function of the effective non-interacting model on the physical orbitals:

$$G_{ij}(t, t') = -i \langle \mathcal{T}_C \hat{c}_i(t) \hat{c}_j^\dagger(t') \rangle_{H_{\text{eff}}}. \quad (10)$$

With this simple construction, the inversion of the Dyson equation can be avoided in favor of a Markovian time propagation within a non-interacting model.

As a successful benchmark, an interaction quench in an inhomogeneous Hubbard model was treated with nonequilibrium DMFT in Ref. 15 using self-consistent second-order perturbation theory as impurity solver. On the theoretical side, however, it remained an open question if the existence of a Lehmann representation must be postulated or if this is a general property of the nonequilibrium self-energy.

In the following we explicitly derive Eq. (8) for the exact self-energy corresponding to the general, interacting Hamiltonian defined in Eq. (1), i.e., we show that the exact self-energy can always be written in the form of a Lehmann representation. The proposed construction scheme is not only useful

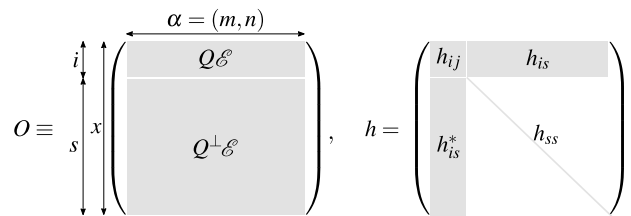


FIG. 2: Unitary completion of the time-dependent Matrix $Q(t)$. The matrix $Q^{\perp}(t)$ contains a completing set of orthonormal basis vectors in its rows. For convenience, the phase factor $\mathcal{E}_{\alpha\alpha'}(t) = \delta_{\alpha\alpha'} \exp(-i\varepsilon_{\alpha}t)$ is also absorbed into $O(t)$. The generating, Hermitian matrix $h(t)$ (cf. Eq. (12)) can be assumed to be diagonal in the virtual sector.

as an analytical tool but also well suited for numerical applications where an approximate self-energy is obtained from a small reference system using exact diagonalization. In this case the number of virtual orbitals is constant and the effort for solving Eq. (7) scales linearly in t_{max} . This is a great advantage if one is interested in long-time dynamics.

B. Explicit construction

We start our construction from the Lehmann representation of G as stated in Eq. (3). For our model Hamiltonian (1) the associated one-particle excitation energies ε_{α} and the Q -matrix are given by Eq. (5). The self-energy is related to this representation through Dyson's equation $\Sigma = G_0^{-1} - G^{-1}$. However, the inverse G^{-1} cannot directly be calculated with Eq. (3) since $Q(t)$ is not quadratic. As a first step we block up the matrix $Q(t)$ to a quadratic form. This is achieved by interpreting its orthonormal rows (cf. Eq. (6)) as an incomplete set of basis vectors. $Q(t)$ itself is an incomplete unitary transform from this viewpoint. We now pick an arbitrary, pairwise orthonormal completion of this basis to find an unitary transform $O(t)$ that contains $Q(t)$ in its upper block (cf. Fig. 2). The next steps of our discussion will be independent of the particular completion that is chosen. The only mathematical requirement is that it is as smooth (and thus differentiable) in the time variable t as $Q(t)$; see Appendix A for numerical details on the construction of $O(t)$.

The completed unitary transform $O(t)$ describes additional virtual orbitals (labeled by the index s , see Fig. 2 and Eq. (9)). For convenience, we also absorb in the definition of $O(t)$ the extra factor $\mathcal{E}_{\alpha\alpha'}(t) = \delta_{\alpha\alpha'} \exp(-i\varepsilon_{\alpha}t)$ that stems from the non-interacting Green's function $g(\varepsilon_{\alpha}; t, t)$ (cf. Eqs. (3) and (4)). For clarity in the notations we use the following index convention throughout this paper

$$\begin{aligned} \text{physical orbitals: } & i, j, & \text{virtual orbitals: } & r, s, \\ \text{physical or virtual orbitals: } & x, y, & \text{excitations: } & \alpha, \alpha'. \end{aligned} \quad (11)$$

Like every time-dependent unitary transform, $Q(t)$ is generated by an associated Hermitian matrix. We define

$$h_{xy}(t) = \sum_{\alpha} [i\partial_t O_{x\alpha}(t)] O_{\alpha y}^{\dagger}(t). \quad (12)$$

Indeed, by integration we have

$$O(t) = \mathcal{T} \exp \left(-i \int_0^t h(t') dt' \right) O(0) \quad (13)$$

and furthermore $h(t)$ is Hermitian:

$$\begin{aligned} h(t) &= [i\partial_t O(t)] O^\dagger(t) = i\partial_t [O(t) O^\dagger(t)] - O(t) i\partial_t O^\dagger(t) \\ &= ([i\partial_t O(t)] O^\dagger(t))^\dagger = h^\dagger(t). \end{aligned} \quad (14)$$

We now require the virtual part $h_{ss'}(t)$ to be diagonal and time-independent, i.e., $h_{ss'}(t) = h_{ss}(0) \delta_{ss'}$. To this end we use our freedom in choosing the completing basis vectors $Q^\perp(t)$ which allows us to perform the associated unitary transform in the virtual sector (see Fig. 2). With the resulting $h_{xy}(t)$ we define the single-particle Hamiltonian $H_{\text{eff}}(t)$

$$H_{\text{eff}}(t) = \sum_{xy} h_{xy}(t) c_x^\dagger c_y, \quad (15)$$

which has precisely the form of the effective Hamiltonian stated in Eq. (9). The requirement of a diagonal virtual sector defines the effective Hamiltonian uniquely up to rotations in invariant subspaces.

At time $t = 0$, the effective medium can be stated in a diagonal form which is useful for the evaluation of the corresponding one-particle Green's function. We recall that we required $O(t)$ to be as smooth as $Q(t)$ and take a look at

$$[i\partial_t O(t)]_{t=0} = h(0)O(0) = O(0)M, \quad (16)$$

where $M = O^\dagger(0)h(0)O(0)$. Eq. (16) implies in particular that $[i\partial_t Q(t)\mathcal{E}(t)]_{t=0} = Q(0)M$ (cf. Fig. 2). However, from Eq. (5) one easily evaluates $[[i\partial_t Q(t)\mathcal{E}(t)]_{i\alpha}]_{t=0} = Q(0)_{i\alpha} \varepsilon_\alpha$ and we can thus identify $M_{\alpha\alpha'} = \delta_{\alpha\alpha'} \varepsilon_\alpha$. Putting everything together we find

$$h_{xy}(0) = \sum_\alpha O_{x\alpha}(0) \varepsilon_\alpha O_{y\alpha}^*(0). \quad (17)$$

We require that the effective medium is initially in thermal equilibrium with the same inverse temperature β and the same chemical potential μ as the physical system. The associated one-particle Green's function of the medium is defined as

$$F_{xy}(t, t') = -i \langle \mathcal{T}_C \hat{c}_x(t) \hat{c}_y^\dagger(t') \rangle_{H_{\text{eff}}}. \quad (18)$$

Recalling the diagonal form of the effective medium at $t = 0$ (cf. Eq. 17) and using that the effective Hamiltonian (15) is non-interacting, we can easily rewrite this expression into

$$F_{xy}(t, t') = i \sum_\alpha O_{x\alpha}(t) [f(\varepsilon_\alpha) - \Theta_C(t, t')] O_{y\alpha}^*(t). \quad (19)$$

The physical sector of F is by construction identical with the Lehmann representation of G :

$$F_{ij}(t, t') = \sum_\alpha Q_{i\alpha}(t) g(\varepsilon_\alpha; t, t') Q_{j\alpha}^*(t') = G_{ij}(t, t'). \quad (20)$$

F encodes the full information on the one-particle excitations of the system defined by the Hamiltonian (1). Eq. (20) further stresses the fact that in principle any (sufficiently smooth)

completion of $Q(t)$ to a unitary transform $O(t)$ leads to a valid effective Hamiltonian. The physical sectors of $O(t)$ and $h(t)$ remain independent of its choice. The virtual sectors, on the other hand, are affected and only the special choice of $O(t)$ (cf. the discussion above and below Eq. (15)) guarantees a diagonal form of the effective medium.

Having found an effective, non-interacting model that reproduces the correct Green's function, it remains to link this back to the self-energy. The time-non-local (correlated) part $\Sigma_{ij}^C(t, t')$ follows by tracing out the virtual orbitals. This procedure is straightforward as they are all non-interacting and we can use, e.g., a cavity-like ansatz¹⁷ or an equation of motion based approach.¹⁵ This results in a hybridization-like function

$$\Sigma_{ij}^C(t, t') \equiv \sum_s h_{is}(t) g(h_{ss}; t, t') h_{js}^*(t') \quad (21)$$

that encodes the influence of the virtual sites on the physical sector. The Green's function at the physical orbitals is then obtained from a Dyson-like equation

$$F_{ij}(t, t') = \left[\frac{1}{F_0^{-1} - \Sigma^C} \right]_{ij}(t, t'), \quad (22)$$

where

$$[F_0^{-1}]_{ij}(t, t') = [i\partial_t - h_{ij}(t)] \delta_C(t, t'), \quad (23)$$

with $\delta_C(t, t') = \partial_t \Theta_C(t, t')$ as the contour delta function.

To make the final connection to the self-energy we evaluate the physical sector of h . With

$$\begin{aligned} i\partial_t Q_{i(m,n)}(t) e^{-i\varepsilon_{(m,n)}t} &= z_{(m,n)} \langle m | [\hat{c}_i(t), \hat{H}(t)] | n \rangle \\ &= \sum_j (T_{ij}(t) - \mu \delta_{ij}) Q_{j(m,n)}(t) \\ &\quad + \sum_{j'j''} U_{ij'j''}(t) z_{(m,n)} \langle m | \hat{c}_{j'}^\dagger(t) \hat{c}_{j''}(t) | n \rangle \end{aligned} \quad (24)$$

we obtain

$$\begin{aligned} h_{ij}(t) &= T_{ij}(t) - \delta_{ij} \mu + \Sigma_{ij}^{\text{HF}}(t), \\ \Sigma_{ij}^{\text{HF}}(t) &\equiv 2 \sum_{j'j''} U_{ij'j''}(t) \langle \mathcal{T}_C \hat{c}_{j'}^\dagger(t) \hat{c}_{j''}(t) \rangle_{H_{\text{eff}}}. \end{aligned} \quad (25)$$

At the physical orbitals the effective Hamiltonian is thus determined by the Hartree-Fock Hamiltonian. By comparison of Eq. (22) with the Dyson equation

$$G_{ij}(t, t') = \left[\frac{1}{G_0^{-1} - \Sigma} \right]_{ij}(t, t'), \quad (26)$$

where

$$[G_0^{-1}]_{ij}(t, t') = [i\partial_t - (T_{ij}(t) - \mu \delta_{ij})] \delta_C(t, t'), \quad (27)$$

we finally identify

$$\Sigma_{ij}(t, t') = \delta_C(t, t') \Sigma_{ij}^{\text{HF}}(t) + \Sigma_{ij}^C(t, t'), \quad (28)$$

concluding our construction of the self-energy. Let us stress that with Eqs. (15), (21) and (25) we now have an *explicit* recipe to construct the Lehmann representation of the self-energy. This representation is further unique as follows from the uniqueness of the corresponding effective Hamiltonian (cf. the discussion above and below Eq. (15)).

C. Useful properties

With the Hamiltonian of the effective medium, Eq. (15), at hand, a number of useful properties follow immediately:

1. Positive spectral weight

By taking a look at the Matsubara branch only, one can link the Lehmann representation of the self-energy to the positive definiteness of its equilibrium spectral function. With $\Sigma^M(\tau - \tau') \equiv -i\Sigma(-i\tau, -i\tau')$ we can perform the usual Fourier transform from imaginary time to Matsubara frequencies and then find the analytical continuation $\Sigma^M(\omega)$ to the complex-frequency plane (see for example Ref. 17). The spectral function is defined as

$$C_{ij}^\Sigma(\omega) = \frac{i}{2\pi} [\Sigma_{ij}^M(\omega + i0) - \Sigma_{ij}^M(\omega - i0)] \quad (29)$$

for real ω . This can explicitly be calculated from the parameters of the effective Hamiltonian. One finds:

$$C_{ij}^\Sigma(\omega) = \sum_s h_{is}(0) h_{js}^*(0) \delta(\omega - h_{ss}), \quad (30)$$

where $\delta(\omega)$ is the Dirac delta function. The positive definiteness for every ω is immediately evident.

2. Higher-order correlation functions

The self-energy and its time derivatives can be used to calculate certain expectation values of higher order. Prominent examples include the interaction energy or the local double occupation. Their calculation is based on the evaluation of contour integrals of the form $\int_C d\tilde{t} \Sigma(t, \tilde{t}) G(\tilde{t}, t')$. By comparing the equations of motion for $G_{ij}(t, t')$ and $F_{xy}(t, t')$ one readily finds the identity

$$\int_C d\tilde{t} \sum_j \Sigma_{ij}(t, \tilde{t}) G_{j\tilde{t}}(\tilde{t}, t') = \sum_j [h_{ij}(t) - T_{ij}(t)] F_{j\tilde{t}}(t, t') + \sum_s h_{is}(t) F_{s\tilde{t}}(t, t'). \quad (31)$$

This is a remarkable relation as the contour integration can be avoided in favor of a simple matrix multiplication.

3. Quantum quenches

A convenient tool to drive quantum systems out of equilibrium is given by the so-called quantum quenches. Here, one (or more) parameters of the system are changed suddenly. This sudden change reflects itself as a discontinuous time dependence of the effective Hamiltonian: Assume that the system is subjected to a quench at time $t = 0$, so that $H_{\text{ini}} \rightarrow H_{\text{final}} = \text{const}$. Initially the system is in thermal equilibrium and the effective Hamiltonian is given by Eq. (17),

where ε_α are the excitations energies of H_{ini} . The O -matrix is continuous at $t = 0$ despite the quantum quench (it only depends on $\hat{c}_i(t)$, cf. Eq. (5)). Its time derivative, however, is not and thus $h(t)$ jumps from $h(0)$ to

$$h_{ij}(0^+) = \sum_\alpha [i\partial_t O_{i\alpha}(t)]_{t=0^+} O_{j\alpha}^*(0). \quad (32)$$

After this jump, the effective Hamiltonian will in general not be constant for times $t > 0$, i.e., $h(t) \neq h(0^+)$.

IV. APPLICATION TO CLUSTER-PERTURBATION THEORY

The simplest numerical application of our formalism is given by cluster-perturbation theory^{7,9,19-22} (CPT). The idea of CPT is to split the system into small clusters which can be treated by means of exact-diagonalization techniques. The cluster self-energies are then used as approximate input for the Dyson equation (7) to obtain the CPT Green's function. The same concept is part of more powerful approaches like DMFT^{5,6,28,29} or self-energy functional theory^{10,30} where the CPT Green's function is self-consistently or variationally linked to the self-energy of a reference system. The following construction of an effective Hamiltonian for CPT applies to such techniques as well.

A. Cluster-perturbation theory (CPT)

From now on we restrict ourselves to the fermionic Hubbard model. The locality of its interaction term allows us to cast its Hamiltonian into the following form:

$$H(t) = \sum_I \underbrace{\left[\sum_{ij\sigma} [T_{ij\sigma}^I(t) - \mu \delta_{ij}] c_{i\sigma}^\dagger c_{j\sigma} + U(t) \sum_i n_{i\uparrow} n_{i\downarrow} \right]}_{\text{cluster system } H_I} + \underbrace{\sum_{I \neq J} \sum_{ij\sigma} T_{ij\sigma}^{IJ}(t) c_{i\sigma}^\dagger c_{j\sigma}}_{\text{inter-cluster hopping}}. \quad (33)$$

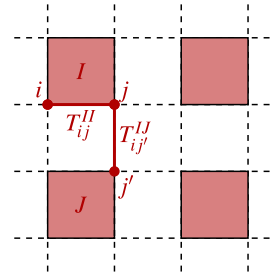


FIG. 3: Illustration of the partitioning of an infinite, two-dimensional square lattice into 2×2 clusters. The sites i, j lie within the same cluster I , j' belongs to a different cluster J . The cluster diagonal part of the hopping matrix T_{ij}^{II} describes the intra-cluster, the cluster off-diagonal part $T_{jj'}^{IJ}$ ($I \neq J$) the inter-cluster-hopping.

Here, the indices I, J label the cluster systems, while the indices i, j run over the sites within a cluster only (see Fig. 3). Of course, this is fully equivalent with the usual form of the Hubbard model which is re-obtained by combining (I, i) to a superindex, i.e., $(I, i) \rightarrow i$. The operator $n_{Ii\sigma} = c_{Ii\sigma}^\dagger c_{Ii\sigma}$ measures the particle density with spin projection $\sigma = \uparrow, \downarrow$. The Green's function of the isolated cluster I with intra-cluster Hamiltonian H_I is

$$G_{ij\sigma}^I(t, t') = -i \langle \mathcal{T}_C \hat{c}_{Ii\sigma}(t) \hat{c}_{Ij\sigma}^\dagger(t') \rangle_{H_I}, \quad (34)$$

so that

$$[G^I]_{ij\sigma}^{-1}(t, t') = [i\partial_t - (T_{ij\sigma}^I(t) - \mu\delta_{ij})] \delta_C(t, t') - \Sigma_{ij\sigma}^I(t, t'), \quad (35)$$

where Σ^I denotes the corresponding self-energy. We further define

$$G' = \begin{pmatrix} G^1 & 0 & \cdots \\ 0 & G^2 & \cdots \\ \vdots & \vdots & \ddots \end{pmatrix}, \quad \Sigma' = \begin{pmatrix} \Sigma^1 & 0 & \cdots \\ 0 & \Sigma^2 & \cdots \\ \vdots & \vdots & \ddots \end{pmatrix}. \quad (36)$$

With the inter-cluster (ic) hopping $[T^{\text{ic}}]_{ij\sigma}^{II} = (1 - \delta_{IJ})T_{ij\sigma}^{II}$ the CPT Green's function is defined as

$$G^{\text{CPT}} \equiv \frac{1}{(G')^{-1} - T^{\text{ic}}} = \frac{1}{G_0^{-1} - \Sigma'}, \quad (37)$$

where $[G_0^{-1}]_{ij\sigma}^{II}(t, t') = [i\partial_t - (T_{ij\sigma}^{II}(t) - \mu\delta_{IJ}\delta_{ij})] \delta_C(t, t')$. The definition of G^{CPT} reveals that CPT becomes exact in the limit of vanishing interaction. We then have $\Sigma' = 0$ and thus $G^{\text{CPT}} = [G_0^{-1}]^{-1} = G_0$. Solving Eq. (37) in case of non-vanishing Σ' , on the other hand, requires the solution of a Dyson equation. This brings us back to our original problem.

B. Application of the Lehmann representation for the self-energy

Using our results from Sec. III we can avoid the solution of the Dyson equation and rather decompose the self-energies of the isolated clusters into their Lehmann representations:

$$\begin{aligned} \Sigma_{ij\sigma}^I(t, t') &= \delta_C(t, t') [\Sigma^{\text{HF}}]_{ij\sigma}^I(t) \\ &+ \sum_s h_{is\sigma}^I(t) g(h_{ss\sigma}^I; t, t') [h^I]_{js\sigma}^*(t'). \end{aligned} \quad (38)$$

Here, $h^I(t)$ are the parameters of the effective medium corresponding to the I -th cluster. We define

$$h^I(t) = \begin{pmatrix} h^1(t) & 0 & \cdots \\ 0 & h^2(t) & \cdots \\ \vdots & \vdots & \ddots \end{pmatrix}. \quad (39)$$

It is now straightforward to realize that the inclusion of the inter-cluster hopping by means of Eq. (37) is completely trivial in this language. Namely,

$$h^{\text{CPT}}(t) = h^I(t) + T^{\text{ic}}(t). \quad (40)$$

With

$$H^{\text{CPT}}(t) = \sum_{IJ} \sum_{xy\sigma} [h^{\text{CPT}}]_{xy\sigma}^{IJ} c_{Ix\sigma}^\dagger c_{Jy\sigma}, \quad (41)$$

we then have

$$[G^{\text{CPT}}]_{ij\sigma}^{II}(t, t') = -i \langle \mathcal{T}_C \hat{c}_{Ii\sigma}(t) \hat{c}_{Jj\sigma}^\dagger(t') \rangle_{H^{\text{CPT}}}. \quad (42)$$

While this is an easy and intuitive description, we remark that $h^I(t)$ includes virtual orbitals. The inter-cluster hopping $T^{\text{ic}}(t)$, on the other hand, is defined solely in the physical sector and has to be blocked up accordingly ($[T^{\text{ic}}(t)]_{rs\sigma}^{II} = [T^{\text{ic}}(t)]_{is\sigma}^{II} = [T^{\text{ic}}(t)]_{rs\sigma}^{II} = 0$).

As an important observable we briefly discuss the calculation of the total energy within CPT. While the kinetic energy follows straightforwardly from the one-particle density matrix as $E_{\text{kin}}(t) = -i \sum_{IJ} \sum_{ij\sigma} T_{ij\sigma}^{IJ} G_{ij\sigma}^{IJ}(t, t^+)$, the interaction energy can only be accessed indirectly through the self-energy. It is given by

$$E_{\text{int}}(t) = -i \sum_{ij} \int_C dt_1 \Sigma_{ij\sigma}^I(t, t_1) G_{ji\sigma}^{\text{CPT}}(t_1, t^+). \quad (43)$$

The evaluation of this contour-integral in Eq. (43) is straightforward within our formalism by using Eq. (31).

V. NUMERICAL RESULTS

A. Prethermalization

The study of real-time dynamics initiated by an interaction quench in the Hubbard model has attracted much attention recently.³²⁻³⁸ Here, the system is prepared in a thermal (usually non-interacting) initial state and then, after a sudden change of the interaction parameter U , evolves in time as prescribed by the interacting Hamiltonian. While the setup is apparently simple, the search for universal properties of the time evolution remains notoriously difficult due to the non-integrability of the Hubbard model in two and higher dimensions. Apart from the general assumption that non-integrable models feature thermalization and thus lose memory of the initial state in the long-time limit,³⁹ only the time evolution after quenches to a weak, finite Hubbard U seems to be well understood so far. Here, it could be shown by means of weak-coupling perturbation theory^{37,38,40,41} that observables initially relax to non-thermal, quasistationary values (the system prethermalizes) before the significantly slower relaxation towards the thermal values sets in.

It was later worked out⁴² that the mechanism which traps the system in a quasi-stationary prethermal state is quite similar to the mechanism that hinders non-interacting systems from thermalizing. In the latter case the integrability of the Hamiltonian leads to a large number of constants of motion that highly constrain the dynamics of the system. In case of weakly interacting systems it is the proximity to the integrable point that introduces approximate constants of motion and hinders relaxation beyond the prethermalization plateau

on short timescales $t \lesssim T/U^2$ (here, T is the nearest-neighbor hopping). Relaxation towards the thermal average is delayed until later times ($t \gtrsim T^3/U^4$).

As a proof of concept of our formalism we use nonequilibrium CPT to investigate the short- and long-time dynamics of an inhomogeneous initial state after an interaction quench in the Hubbard model. In particular we will study if and to what extent the CPT is able to describe prethermalization and the subsequent relaxation to a thermal state.

B. Setup

We consider the Hubbard model at zero temperature ($\beta \rightarrow \infty$) and half-filling ($\mu = U/2$) on a square lattice of $L = 10 \times 10$ sites with periodic boundary conditions. Cluster indices run over $I, J \in \{0, 1, \dots, 24\}$ and $i, j \in \{0, 1, 2, 3\}$, so that the system is cut into 25 clusters of size 2×2 . The hopping is restricted to nearest neighbors and we set $T = 1$ to fix energy and time units. Translational invariance of the initial state is broken by applying a local magnetic field of strength B to an arbitrarily chosen ‘‘impurity site’’ (here, site 0 in cluster 0):

$$T_{ij\sigma}^{IJ}(t) = \delta_{\langle(I,t),(J,j)\rangle} T - z_\sigma \delta_{I,J} \delta_{i,j} \delta_{I,0} \delta_{i,0} B(t), \quad (44)$$

where $\delta_{\langle \dots \rangle}$ is non-zero and unity for nearest neighbors only and where $z_\uparrow = +1$ and $z_\downarrow = -1$. Initially, the magnetic field is switched on with strength $B(0) = 10$ to induce a (nearly) fully polarized magnetic moment on the impurity site and then switched off for times $t > 0$:

$$B(t) = B(0)(1 - \Theta(t)). \quad (45)$$

Here, $\Theta(t)$ is the Heaviside step function. Furthermore, the interaction $U(t)$ is switched off initially and then switched on to a non-zero value U_{fin}

$$U(t) = U_{\text{fin}} \Theta(t). \quad (46)$$

Hence, in the quantum quench considered here, two parameters are changed simultaneously. The initial Hamiltonian H_{ini} features no interactions but is inhomogeneous due to the local magnetic field, the final Hamiltonian H_{fin} is translationally invariant due to the absence of the magnetic field but has a finite interaction $U_{\text{fin}} > 0$.

To apply nonequilibrium CPT, we use exact diagonalization to solve the 25 independent cluster problems and to construct the Hamiltonian of the effective medium (for details on the numerical implementation see Appendix A). Finally, Eq. (40) is used to account for the inter-cluster hopping. The number of non-zero elements of a cluster’s Q -matrix and therefore the computational effort of our approach increases quadratically with the number of active states in the density matrix $\rho_{\text{cluster}} = \sum_m \exp(-\beta E_m) |m\rangle\langle m| (H_{\text{cluster}} |m\rangle = E_m |m\rangle)$, i.e., states that contribute with a significant weight $\exp(-\beta E_m)$ to thermal averages. For convenience we have therefore chosen a zero-temperature initial state and consider a weak interaction $U = 10^{-4}$ to lift the ground-state degeneracy present in the

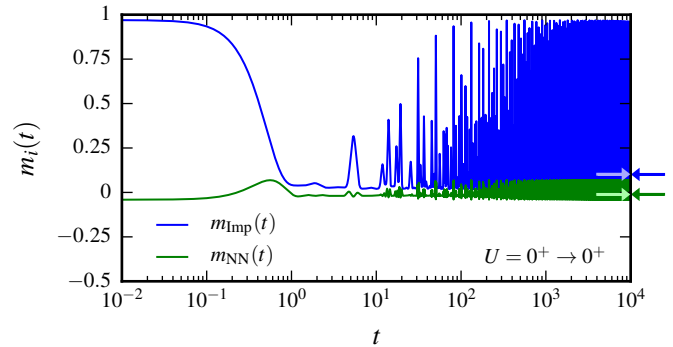


FIG. 4: (Color online) Time evolution of the local magnetic moment at the impurity ($m_{\text{Imp}}(t)$, blue line) and its nearest neighbors ($m_{\text{NN}}(t)$, green line). The dark-blue (dark-green) arrow, which is pointing from right to left, indicates the long time average of the blue (green) curve. The light-blue (light-green) arrow, which is pointing from left to right, indicates the analytical average (47). The long time average was taken over 500,000 data points in the interval $[0.5 \times 10^4, 10^4]$.

non-interacting system (denoted as $U = 0^+$ in the following). The effective Hamiltonian $h^I(t)$ for each cluster is then of size 48×48 and the final CPT Hamiltonian of size 1200×1200 . Exploiting its sparse form we are able to perform 1,000,000 time steps with $\Delta t = 0.01$ to reach a maximal time $t_{\text{max}} = 10^4$ with modest computational effort. For comparison we note that prior studies based on the nonequilibrium CPT, e.g. Refs. 7,22, have been limited to $t_{\text{max}} = 10$ –20 inverse hoppings.

The partitioning of the lattice into 2×2 clusters by CPT breaks rotational and reflection symmetries of the original problem. These are restored by averaging the resulting one-particle density matrix over the 4 possible ways to cut the lattice into 2×2 clusters. In the following we will show results for the time evolution of the local magnetic moment $m_i(t) = n_{i\uparrow}(t) - n_{i\downarrow}(t)$ at the impurity ($m_{\text{Imp}}(t)$) and at its nearest neighbors ($m_{\text{NN}}(t)$). Only the latter are affected by the averaging. It restores the equivalence of nearest neighbors that lie in the same and nearest neighbors that lie in a neighboring cluster of the impurity. The extensive quantities total energy $E_{\text{tot}}(t) = E_{\text{kin}}(t) + E_{\text{int}}(t)$ (cf. Eq. (43) and preceding discussion) and total magnetization $M(t) = \sum_i m_i(t)$ are both unaffected by the averaging.

The initial state is the same for all quenches discussed in the following. We find a polarization of $m_{\text{Imp}}(0) \approx 0.97$ at the impurity which is partially screened (e.g., $m_{\text{NN}}(0) = -0.04$) so that the total magnetization amounts to $M(0) = \sum_i m_i(0) \approx 0.70$.

C. Noninteracting case

We first discuss the non-interacting case, i.e., a purely magnetic quench where $U_{\text{fin}} = 0^+$. Here, CPT predicts the exact time evolution (cf. the discussion below Eq. (37)) since the cluster self-energies Σ^I vanish. Our results are shown in Fig. 4. For short times ($t \in [10^{-2}, 4 \times 10^0]$) the local magnetic moment at the impurity $m_{\text{Imp}}(t)$ (blue line) decays to a

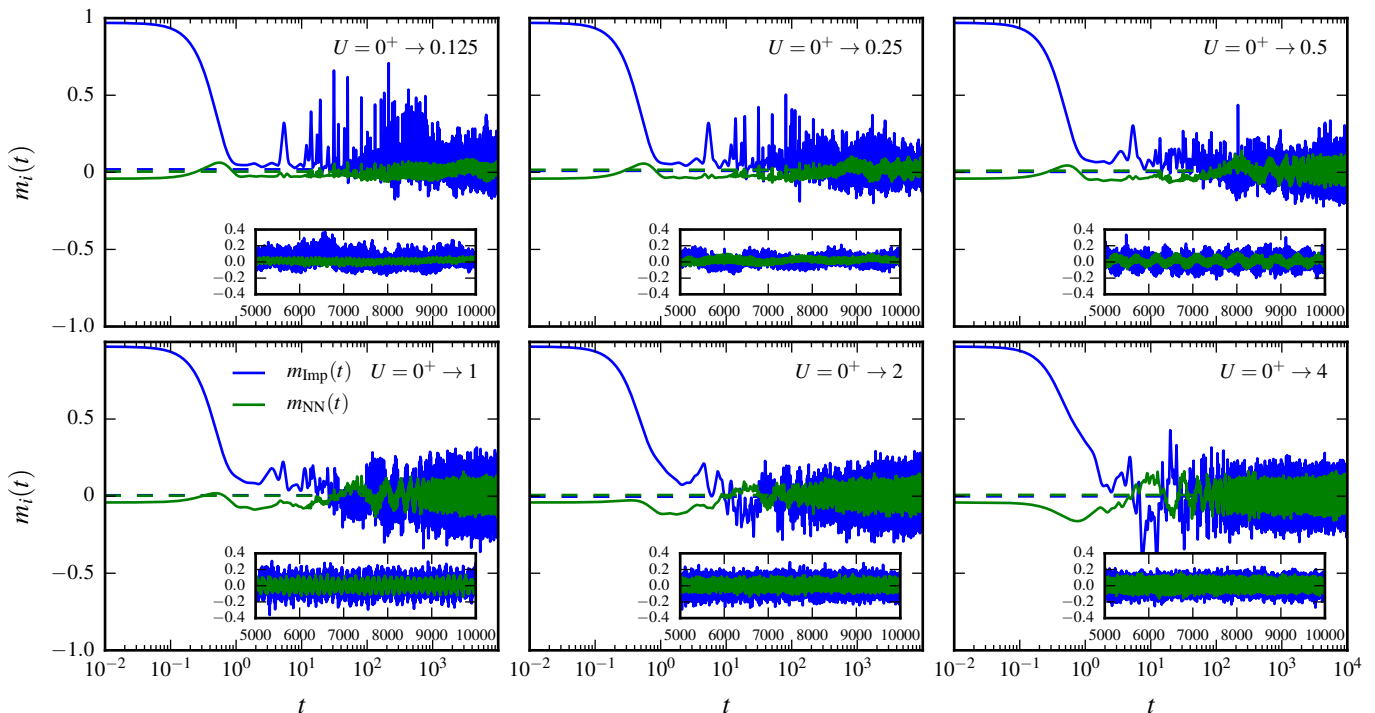


FIG. 5: (Color online) CPT results for the time evolution of the local magnetic moment at the impurity ($m_{\text{Imp}}(t)$, blue line) and at its nearest neighbors ($m_{\text{NN}}(t)$, green line) for quenches from the limit of vanishing interaction $U = 0^+$ (numerically implemented by setting $U = 0.0001$) to finite U_{fin} . In the insets the long-time behavior ($t \in [5 \times 10^3, 10^4]$) is plotted on a linear scale. The interval consists of 500,000 data points and was also used to calculate the long-time average (straight dashed lines). In total 1,000,000 time steps were performed with $\Delta t = 0.01$ on a $L = 10 \times 10$ lattice (cut into 25 clusters of size 2×2 by CPT).

value slightly above zero. Subsequently ($t \in [4 \times 10^0, 10^4]$) the dynamics is governed by collapse-and-revival oscillations caused by the finite system size. In particular we find that $m_{\text{Imp}}(t)$ returns arbitrarily close to its initial value for large times. This is readily understood from the fact that the system's dynamics is governed by the one-particle propagator $\exp(-iT_{\text{fin}}t)$ where T_{fin} denotes the final hopping matrix (i.e., after the quench). T_{fin} involves only a small number of different one-particle energy levels and thus $U(t,0)$ returns arbitrarily close to the identity matrix over time.

For the non-interacting system it is possible to directly access the long-time average of the one-particle density matrix. One finds

$$\begin{aligned} \rho_{ij\sigma}^{\text{avg}} &= \lim_{t_{\text{max}} \rightarrow \infty} \frac{1}{t_{\text{max}}} \int_0^{t_{\text{max}}} dt \langle \hat{c}_{i\sigma}^\dagger(t) \hat{c}_{j\sigma}(t) \rangle \\ &= \frac{1}{L} \sum_{\vec{k}, \vec{k}'} \delta_{\vec{k}, \vec{k}'} e^{i(\vec{k} \cdot \vec{R}_i - \vec{k}' \cdot \vec{R}_j)} \langle \hat{c}_{\vec{k}\sigma}^\dagger(0) \hat{c}_{\vec{k}'\sigma}(0) \rangle, \end{aligned} \quad (47)$$

where we used that H_{fin} can be diagonalized by a Fourier transformation involving the reciprocal lattice vectors \vec{k} (\vec{R}_i denotes the lattice vector to site i). We then have $H_{\text{fin}} = \sum_{\vec{k}\sigma} \varepsilon_{\vec{k}} \hat{c}_{\vec{k}\sigma}^\dagger \hat{c}_{\vec{k}\sigma}$ and $\hat{c}_{i\sigma}(t) = \frac{1}{\sqrt{L}} \sum_{\vec{k}} e^{-i\vec{k} \cdot \vec{R}_i} e^{-i\varepsilon_{\vec{k}} t} \hat{c}_{\vec{k}\sigma}(0)$, where L is the system size. In Fig. 4 this prediction is compared with the numerical time average and indeed shows perfect agreement. It is interesting to note that for non-degenerate energy levels $\varepsilon_{\vec{k}}$ one would have $\rho_{i\sigma}^{\text{avg}} = N_{\sigma}/L$, where N_{σ}

is the total number of particles with spin σ , and therefore $m_i^{\text{avg}} = M(0)/L$. We conclude that degeneracy of energy levels is required to find memory of the initial state encoded in the average local magnetic moments m_i^{avg} .

D. Quenches to finite U_{fin}

For finite U_{fin} CPT becomes an approximation and it is a priori unclear what kind of phenomena it is able to describe. In Fig. 5 we show the long-time evolution for quenches to different U_{fin} . For weak $U_{\text{fin}} \lesssim 0.5$ we find a (prethermalization-like) separation into two different time scales. Initially the time evolution qualitatively follows the non-interacting case, i.e., we see a fast decay of the local moment at the impurity site (blue line) followed by a quasi-stationary region of collapse-and-revival oscillations. For larger times these oscillations decay and the system relaxes into a state characterized by quasi-periodic fluctuations around its long-time average (dashed blue line) which are driven by different frequencies. Taking a look at the U_{fin} dependence of the dynamics we notice that the region of collapse-and-revival oscillations shrinks with increasing U_{fin} and finally vanishes for $U_{\text{fin}} \gtrsim 1$. The system then directly relaxes into a state with fluctuations around its long-time average.

For comparison, also the magnetic moment at the neighbouring sites $m_{\text{NN}}(t)$ is plotted. While its dynamics for short

times must naturally be different from $m_{\text{Imp}}(t)$ due to the inhomogeneous initial state, we would expect a qualitative agreement in the long-time limit if the system thermalizes. However, this is not the case. There remains a clear difference in the amplitude of the fluctuations around the long-time average up to the largest simulated times. Hence we conclude that the system still keeps memory of the initial state and thus does not thermalize.

Having in mind the general discussion on prethermalization in Sec. V A, one can give an intuitive interpretation of these observations based on the effective-medium approach: While the non-interacting system is isolated and its dynamics is constrained through many constants of motion, there is a large number of virtual orbitals coupled to the system in the interacting case. These virtual orbitals act like a surrounding bath. For weak U_{fin} the virtual orbitals are only weakly coupled to the system and their influence is delayed to large times, while initially the dynamics is constrained similar to the non-interacting case. For strong U_{fin} , on the other hand, the coupling is strong and affects the dynamics of the system considerably. However, the number of virtual sites is still too small to allow for a complete dissipation of the information on the initial state into the bath. Therefore, a thermalized state is not reached. For an exact calculation the number of virtual sites would scale exponentially in system size. For CPT, on the other hand, it scales exponentially only in cluster size but linearly in the number of clusters and thus in the system size. Memory of the initial state is therefore retained within the one-particle density matrix and leaves its traces in the magnetic moments as seen in our calculations.

E. Violation of conservation laws

CPT as an approximation lacks any kind of self-consistency and is thus unable to respect the fundamental continuity equations and their corresponding conservation laws.¹⁰ Therefore, one has to expect a violation of energy- or particle-number conservation, for example. Furthermore, in contrast to the equilibrium case where CPT interpolates between the exact limits $U = 0$ and $T = 0$, it yields exact results only for quenches to $U_{\text{fin}} = 0$. The dynamics after a quench to the atomic limit $T_{\text{fin}} = 0$ (with finite $U_{\text{fin}} > 0$) cannot be described exactly due to the non-local entanglement of the initial state. We thus generally expect that the quality of the CPT results degrades with increasing interaction strength.

The numerical results for the total energy, see Fig. 6, confirm this expectation. Energy conservation is respected for $U_{\text{fin}} = 0$, where CPT is exact. With $U_{\text{fin}} > 0$ and increasing, however, a significant time dependence of the total energy sets in earlier and earlier. For $U_{\text{fin}} \gtrsim 1$ energy conservation is violated already for $t \lesssim 10$. Similar results are found for the total magnetization $M = \sum_i (n_{i\uparrow} - n_{i\downarrow})$, cf. Fig. 7. While the magnetization should be constant for all times since neither hopping nor interaction (cf. Eqs. (44) and (46)) involve spin-flip terms, we find such behavior only for short times. For longer times oscillations arise and the conservation of total magnetization is violated. For increasing U_{fin} the oscillations set in earlier

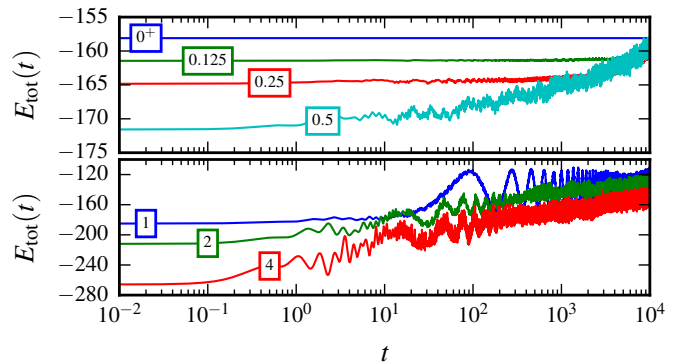


FIG. 6: (Color online) Violation of energy conservation by CPT. The numbers indicate the respective value of U_{fin} . Energy conservation is respected for $U_{\text{fin}} = 0^+$ where CPT is exact (blue line). An increasingly significant violation of energy conservation is seen for larger U_{fin} .

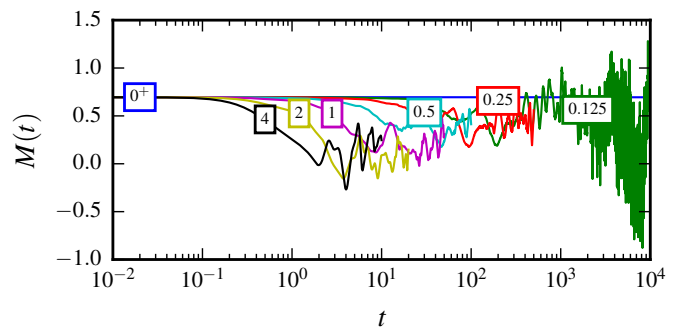


FIG. 7: (Color online) Violation of conservation of total magnetization M by CPT. The numbers indicate the value of U_{fin} . Curves for $U_{\text{fin}} \geq 0.25$ are only partially plotted for better visibility.

indicating again that the quality of CPT is best for values of U_{fin} close to zero.

We note that the total particle number $N = N_{\uparrow} + N_{\downarrow}$, however, is conserved during the time evolution. This holds true for a half-filled and homogeneously charged system and is due to the fact that CPT preserves particle-hole symmetry. This can easily be understood as follows: Each cluster Hamiltonian is particle-hole symmetric and since each cluster is solved exactly within CPT the corresponding effective Hamiltonian $h^l(t)$ is also particle-hole symmetric. The CPT Hamiltonian is now given by Eq. (40) which additionally includes the inter-cluster hopping. However, the inter-cluster hopping is clearly particle-hole symmetric and so is the final CPT Hamiltonian.

VI. SUMMARY AND OUTLOOK

Concluding, we have shown that the nonequilibrium self-energy of an interacting lattice-fermion model can uniquely be decomposed into a superposition of noninteracting, isolated modes. This decomposition is a direct analog to a well-established decomposition of equilibrium Green's functions, called the *Lehmann representation*. Our proof not only provides a direct scheme to construct the Lehmann representation

of the self-energy, and thus allows for a deeper theoretical understanding of the self-energy complementary to its diagrammatic definition, but also proves useful for practical applications.

As a proof of concept we investigated the time evolution of local magnetic moments in the fermionic Hubbard model after an interaction quench using nonequilibrium cluster-perturbation theory. Our formalism allowed to avoid the solution of an inhomogeneous Dyson equation on the Keldysh contour and we were able to propagate the one-particle density matrix up to times $t_{\max} = 10^4$.

On the physical side, quenches to weak U_{fin} turned out to be most interesting. In agreement with the predictions of general perturbative considerations,^{37,38,40–42} we found a separation of the dynamics into two time scales. While the system qualitatively follows the constrained dynamics of the non-interacting $U_{\text{fin}} = 0$ limit, the constraints are broken up for large times due to the interaction and the system shows signs of relaxation. However, memory of the initial state persists in the density matrix up to the largest simulated times clearly indicating the absence of thermalization.

While the simple treatment of correlations by nonequilibrium CPT has shown to be enough to cover the mentioned two-stage relaxation dynamics, it also leads to a violation of the fundamental conservation laws of energy and total magnetization. This could be fixed by additionally imposing a self-consistency condition as it is done in nonequilibrium DMFT or in self-energy functional theory. Due to the significant, additional complexity of these approaches, however, simulations would again be restricted to short time scales. A simpler, more pragmatic approach might thus be preferable where, for example, local continuity equations are enforced to ensure energy, total magnetization and particle-number conservation.¹⁰ Such a ‘‘conserving cluster-perturbation theory’’ could allow for a complete dissipation of initial perturbations and thus total loss of the memory of the initial state. Work along these lines is in progress.

Acknowledgments

We thank Roman Rausch for providing an exact-diagonalization solver for the Hubbard model, Felix Hofmann for a reference implementation of nonequilibrium CPT, and Martin Eckstein and Karsten Balzer for helpful discussions. This work has been supported by the excellence cluster ‘‘The Hamburg Centre for Ultrafast Imaging - Structure, Dynamics and Control of Matter at the Atomic Scale’’ and by the Sonderforschungsbereich 925 (project B5) of the Deutsche Forschungsgemeinschaft. Numerical calculations were performed on the PHYSnet computer cluster at the University of Hamburg.

Appendix A: Numerical construction of the effective Hamiltonian

1. The Q -matrix and its time derivatives

We assume that a small cluster is solved using exact diagonalization and that all time derivatives $H^{(n)}(t) = \partial_t^n H(t)$ of the Hamiltonian are known analytically. The numerical evaluation of Eq. (5) for the Q -matrix is straightforward within exact diagonalization. Its n -th derivative can be obtained as follows. We have

$$\begin{aligned} U^{(n)}(t, 0) &= \partial_t^{n-1}(-iH(t)U(t, 0)) \\ &= -i \sum_{k=0}^{n-1} \binom{n-1}{k} H^{(k)}(t) U^{(n-1-k)}(t, 0) \end{aligned} \quad (\text{A1})$$

for the propagator $U(t, 0)$. The n -th derivative $U^{(n)}(t, 0)$ can then be calculated iteratively as it only depends on $U^{(k)}(t, 0)$ with $k < n$. Using further that

$$\partial_t^n \hat{c}_i(t) = \sum_{k=0}^n \binom{n}{k} U^{(k)}(t, 0) c_i [U^{(n-k)}(t, 0)]^\dagger, \quad (\text{A2})$$

one finds the n -th derivative $\hat{c}_i^{(n)}(t)$ of the annihilation operator and thus of $Q^{(n)}(t)$, see Eq. (5). In the following we will assume that $Q^{(n)}(t)$ is available to arbitrary order.

2. Construction of the effective Hamiltonian at $t = 0$

We start by constructing $Q^\perp(0)$, i.e., a basis for the virtual sector. It is easy to verify that

$$P_{\alpha\alpha'} = \sum_i Q_{i\alpha}^*(0) Q_{i\alpha'}(0), \quad (\text{A3})$$

defines a projector. Diagonalization of P yields the eigenvalues 0 and 1. Eigenvectors corresponding to 1 are given by $Q(0)^\dagger$ itself, eigenvectors corresponding to 0 form the desired matrix $[Q^\perp(0)]^\dagger$. Initially, the effective medium is in equilibrium and thus explicitly given by Eq. (17) at $t = 0$. However, since we picked the completing basis vectors arbitrarily, we will have $h_{ss'} \neq 0$ for $s \neq s'$, i.e., generally h will not be diagonal in the virtual sector. Explicit diagonalization of h in the virtual sector yields a unitary transform R

$$h_{ss'} = \sum_r R_{sr} d_r R_{rs'}^*. \quad (\text{A4})$$

Replacing $Q^\perp(0) \rightarrow RQ^\perp(0)$, we get $h_{ss'} \rightarrow \delta_{ss'} d_s$, i.e., we have found a completing basis so that h is diagonal in the virtual sector.

3. The time derivatives $h^{(n)}(t)$

Assume that $h(t)$, $Q(t)$, $Q^\perp(t)$ and $Q^{(n \geq 1)}(t)$ are known for an arbitrary time t . This is at least the case for $t = 0$ as we have

seen so far. We recall that we required $h(t)$ to be constant in the virtual sector (cf. discussion below Eq. (14))

$$h_{ss'}(t) = \delta_{ss'} h_{ss}(0) \Rightarrow h_{ss'}^{(n \geq 1)}(t) = 0, \quad (\text{A5})$$

i.e., all time derivatives vanish in the virtual sector. Only the hybridization elements and the physical sector yield non-trivial elements. They follow from Eq. (12) as

$$h_{iy}^{(n)}(t) = i \sum_{k=0}^n \binom{n}{k} \sum_{\alpha} [\partial_t^{k+1} (Q_{i\alpha}(t) e^{-i\varepsilon\alpha t})] [O^{(n-k)}(t)]^{\dagger}_{\alpha y}. \quad (\text{A6})$$

$O^{(n)}(t)$ on the other hand only depends on $h^{(k)}(t)$, and $O^{(k)}(t)$, for $k < n$, as readily follows from

$$\begin{aligned} O^{(n)}(t) &= -i \partial_t^{(n-1)} h(t) O(t) \\ &= -i \sum_{k=0}^{n-1} \binom{n-1}{k} h^{(k)}(0) O^{(n-1-k)}(t). \end{aligned} \quad (\text{A7})$$

It is thus possible to iteratively calculate $O^{(n)}(t)$ and $h^{(n)}(t)$.

4. Propagation of the O -matrix

We assume that $O(t)$ and all derivatives of $h^{(n)}(t)$ are known at some time t and we want to propagate the O -matrix to

$O(t + \Delta t)$. Analytically this can be written as

$$O(t + \Delta t) = \mathcal{T} \left\{ \exp \left(-i \int_t^{t+\Delta t} h(t') dt' \right) \right\} O(t). \quad (\text{A8})$$

Using the Magnus expansion,⁴³ the propagator can be systematically expanded in Δt^n and $h^{(n)}(t)$. Assuming that Δt lies within the convergence radius of the Magnus expansion (this is generally expected to be the case for sufficiently small Δt), we can reduce the propagation error arbitrarily by increasing the order. In practice, an evaluation of the Magnus expansion using commutator-free exponential time propagators⁴⁴ (CFETs) allows for an efficient numerical propagation which takes advantage of the sparse form of the effective Hamiltonian.

Having found $O(t + \Delta t)$, we get $h(t + \Delta t)$ from

$$h_{iy}(t + \Delta t) = i \sum_{\alpha} Q_{i\alpha}^{(1)}(t + \Delta t) e^{-i\varepsilon\alpha t} [O(t + \Delta t)]^{\dagger}_{\alpha y}, \quad (\text{A9})$$

and can thus proceed by calculating $O^{(n)}(t + \Delta t)$ and $h^{(n)}(t + \Delta t)$ completing the circle. We emphasize that the whole procedure is numerically exact, i.e., the error is below machine precision, if Δt is chosen sufficiently small.

-
- ¹ A. Polkovnikov, K. Sengupta, A. Silva, and M. Vengalattore, *Rev. Mod. Phys.* **83**, 863 (2011).
 - ² H. Aoki, N. Tsuji, M. Eckstein, M. Kollar, T. Oka, and P. Werner, *Rev. Mod. Phys.* **86**, 779 (2014).
 - ³ L. V. Keldysh, *J. Exptl. Theoret. Phys.* **47**, 1515 (1964).
 - ⁴ K. S. Thygesen and A. Rubio, *The Journal of Chemical Physics* **126**, 091101 (2007).
 - ⁵ P. Schmidt and H. Monien, arXiv:cond-mat/0202046 (2002).
 - ⁶ J. K. Freericks, V. M. Turkowski, and V. Zlatić, *Phys. Rev. Lett.* **97**, 266408 (2006).
 - ⁷ M. Balzer and M. Potthoff, *Phys. Rev. B* **83**, 195132 (2011).
 - ⁸ C. Jung, A. Lieder, S. Brener, H. Hafermann, B. Baxevanis, A. Chudnovskiy, A. Rubtsov, M. Katsnelson, and A. Lichtenstein, *Ann. Phys.* **524**, 49 (2011).
 - ⁹ M. Knap, W. von der Linden, and E. Arrigoni, *Phys. Rev. B* **84**, 115145 (2011).
 - ¹⁰ F. Hofmann, M. Eckstein, E. Arrigoni, and M. Potthoff, *Phys. Rev. B* **88**, 165124 (2013).
 - ¹¹ A. V. Joura, J. K. Freericks, and A. I. Lichtenstein, *Phys. Rev. B* **91**, 245153 (2015).
 - ¹² P. Lipavský, V. Špička, and B. Velický, *Phys. Rev. B* **34**, 6933 (1986).
 - ¹³ S. Hermanns, N. Schlünzen, and M. Bonitz, *Phys. Rev. B* **90**, 125111 (2014).
 - ¹⁴ S. Weiss, J. Eckel, M. Thorwart, and R. Egger, *Phys. Rev. B* **77**, 195316 (2008).
 - ¹⁵ K. Balzer and M. Eckstein, *Phys. Rev. B* **89**, 035148 (2014).
 - ¹⁶ A. L. Fetter and J. D. Walecka, *Quantum Theory of Many-Particle Systems* (Dover Publications, 2003).
 - ¹⁷ C. Gramsch, K. Balzer, M. Eckstein, and M. Kollar, *Phys. Rev. B* **88**, 235106 (2013).
 - ¹⁸ G. Stefanucci, Y. Pavlyukh, A.-M. Uimonen, and R. van Leeuwen, *Phys. Rev. B* **90**, 115134 (2014).
 - ¹⁹ C. Gros and R. Valentí, *Phys. Rev. B* **48**, 418 (1993).
 - ²⁰ D. Sénéchal, D. Perez, and M. Pioro-Ladrière, *Phys. Rev. Lett.* **84**, 522 (2000).
 - ²¹ D. Sénéchal, D. Perez, and D. Plouffe, *Phys. Rev. B* **66**, 075129 (2002).
 - ²² P. Jurgenowski and M. Potthoff, *Phys. Rev. B* **87**, 205118 (2013).
 - ²³ L. Perfetti, P. A. Loukakos, M. Lisowski, U. Bovensiepen, H. Berger, S. Biermann, P. S. Cornaglia, A. Georges, and M. Wolf, *Phys. Rev. Lett.* **97**, 067402 (2006).
 - ²⁴ I. Bloch, J. Dalibard, and W. Zwerger, *Rev. Mod. Phys.* **80**, 885 (2008).
 - ²⁵ J. Rammer, *Quantum Field Theory of Non-equilibrium States* (Cambridge University Press, Cambridge, UK, 2007).
 - ²⁶ R. van Leeuwen, N. E. Dahlen, G. Stefanucci, C.-O. Almbladh, and U. von Barth, *Introduction to the Keldysh formalism*, vol. 706 of *Lecture Notes in Physics* (Springer, Heidelberg, Germany, 2006).
 - ²⁷ M. Aichhorn, E. Arrigoni, M. Potthoff, and W. Hanke, *Phys. Rev. B* **74**, 235117 (2006).
 - ²⁸ W. Metzner and D. Vollhardt, *Phys. Rev. Lett.* **62**, 324 (1989).
 - ²⁹ A. Georges and G. Kotliar, *Phys. Rev. B* **45**, 6479 (1992).
 - ³⁰ M. Potthoff, *Eur. Phys. J. B* **32**, 429 (2003).
 - ³¹ F. Hofmann, M. Eckstein, and M. Potthoff, arXiv:1510.05866 (2015).
 - ³² C. Kollath, A. M. Läuchli, and E. Altman, *Phys. Rev. Lett.* **98**,

- 180601 (2007).
- ³³ S. Trotzky, Y.-A. Chen, A. Flesch, I. P. McCulloch, U. Schollwöck, J. Eisert, and I. Bloch, *Nat. Phys.* **8**, 325 (2012).
- ³⁴ U. Schneider, L. Hackermüller, J. P. Ronzheimer, S. Will, S. Braun, T. Best, I. Bloch, E. Demler, S. Mandt, D. Rasch, et al., *Nature Physics* **8**, 213 (2012).
- ³⁵ M. Eckstein, M. Kollar, and P. Werner, *Phys. Rev. B* **81**, 115131 (2010).
- ³⁶ M. Eckstein, M. Kollar, and P. Werner, *Phys. Rev. Lett.* **103**, 056403 (2009).
- ³⁷ M. Moeckel and S. Kehrein, *Phys. Rev. Lett.* **100**, 175702 (2008).
- ³⁸ M. Stark and M. Kollar, arXiv:1308.1610 (2013).
- ³⁹ M. Rigol, V. Dunjko, and M. Olshanii, *Nature* **452**, 854 (2008).
- ⁴⁰ M. Moeckel and S. Kehrein, *Annals of Physics* **324**, 2146 (2009).
- ⁴¹ M. Moeckel and S. Kehrein, *New Journal of Physics* **12**, 055016 (2010).
- ⁴² M. Kollar, F. A. Wolf, and M. Eckstein, *Phys. Rev. B* **84**, 054304 (2011).
- ⁴³ S. Blanes, F. Casas, J. Oteo, and J. Ros, *Physics Reports* **470**, 151 (2009).
- ⁴⁴ A. Alvermann and H. Fehske, *Journal of Computational Physics* **230**, 5930 (2011).